# Combination of Information from Several X-Ray Images for Improving Defect Detection Performances – Application to Castings Inspection

Gwenaële LECOMTE, Valérie KAFTANDJIAN, laboratory CNDRI of INSA de Lyon, France
Emmanuelle CENDRE, RISOE National laboratory, Roskilde, Denmark

**Abstract**. The results presented were obtained in the frame of the European QUME[1] project, during which three Non Destructive Techniques were developed to improve inspection of castings : multi-angle radioscopy, X-ray spectrometry and vibration analysis. We present the concept of confidence level (the so-called mass function of the Evidence theory) assigned to the information delivered by each method. A simple model is introduced, based on the deviation of the measurements from the mean of a normal measurement, with respect to the standard deviation. Information is combined using the Dempster rule of combination. The final decision on the sample acceptability can be done in an objective way by a threshold in the confidence level. Results obtained on a set of 171 castings samples, containing 62 defects, show that the combination of images acquired at different angles allow both to detect more defects than a single projection approach, but also that the defects detected present a higher confidence level, thanks to the data fusion step. X-ray spectrometry was not so sensitive as expected, and thus, fusion was done in a cautious way, considering spectrometric results only when fused with radioscopy. Vibration analysis results were not reliable enough to allow a successful data fusion step. However, the potential of the different modalities will be discussed.

## Introduction

Cast components are usually featured by a complex shape with varying thicknesses. For safety parts, a 100 % X-ray inspection is often required. Due to the shape, different X-ray projections are necessary to inspect the sample in a reliable way. Radioscopic devices are now preferred to film radiography in a number of industrial application areas. A key interest is related to the choice of optimum projection while moving the part in front of the detector, usually an image intensifier. Another interest is of course related to the possibility of automatic defect detection and application of standards for defect criticality. However, at present high thicknesses (typically > 40 mm) are difficult to inspect, and defect detection performance by radioscopy is very low in this range. Spectrometry is known to be more adequate for high thicknesses, due to the fact that the detector absorption efficiency is much higher. However, spectrometry is only possible on a limited measurement points due to the acquisition time needed.
The aim of the QUME[1] EU funded project was to improve the inspection performance of cast parts by combining radioscopic imaging and X-ray spectrometry. A third method was

1 QUME is the acronym for the GROWTH RTD project entitled: On-line process and Quality optimisation for the manufacturing of cast MEtallic parts, G1RD-2000-00444. Partners : InnospeXion ApS (DK), Carl Bro A/S (DK), RISOE (DK), Univ. Liverpool (UK), Monition Ltd (UK), ISQ (PT), Stampal Spa (IT), IFG (DE), INSA-CNDRI (FR)

developed in the frame of the project, based on the analysis of the vibration of the sample after a short mechanical excitation. Another part of the project involved the assessment of defect criticality (including destructive mechanical tests) and their correlation to the casting process parameters.

Our study deals with the processing and combination of data coming from the three methods, in order to deliver a unique decision concerning a sample (acceptable / not acceptable) in adequation with the end user specifications (Stampal company). Data were fused using the concept of confidence level or mass distributions developed in the Evidence theory, and the results are presented here. Casting samples were analysed with the three methods (radioscopy, spectrometry and vibration) in one cabinet. The acquisition set-up (machine developed) is out of the scope of this paper.

## MATERIAL AND METHODS

### *Sample*

The studied sample is an aluminium connecting rod (Figure 1) for car manufacturing, produced by thixocasting. This particular sample was selected for its relatively simple shape, adequate for vibration analysis, and for the presence of specific defects in a critical zone (the central arm), which are difficult to detect because of the thick rib. It is expected that the use of the three methods should help the defect detection.

Figure 1 : Aluminium connecting rod for car manufacturing, produced by thixocating (Stampal company) .

171 samples were studied, from two production batches, among which 30 samples are said not acceptable by the manufacturer (Stampal), in accordance with ASTM standard, representing 62 defects. Different defect types have been investigated, mainly shrinkage cavities, gas cavities, with various gravity levels. 1 inclusion and 2 cold junctions were also present. Those defects were reported by a manual X-ray investigation (where the right projection angle and right X-ray energy are manually chosen for each sample). The case of cold junctions is particular, as it is well known that this defect is very hard to detect by X-rays (this is why the choice of the right angle is so important). It was expected that vibration analysis would help the detection of this defect type.

### *Data acquisition*

The Figure 2 illustrates the three techniques used for the same sample. The sample is first examined by radioscopy, using a microfocus X-ray tube and an image intensifier. Four orientations are selected to put the emphasis on the critical areas of the sample. The central part is partly visible in the four views.

The second test is the spectrometry, using a NaI detector. Spectrometry differs from radioscopy in the sense that the detector is an energy dispersive photon counting system. Spectrometric detectors are usually very thick in order to have a good absorption factor. All the transmitted photons are counted independently and separated in energy, so as to get a spectrum of number of photons transmitted versus energy. Three volumes are successively measured by translating the sample. Reference measurements on a known thickness are carried out in between in order to calibrate the X-ray tube drift. Both radioscopy and spectrometry acquisition conditions were optimised by the RISOE National Laboratory, some details can be found in [1].
The third acquisition consists of the vibration analysis using two accelerometers placed on both extremities of the sample. Eleven successive spectra are measured after knocking the sample with an hammer of calibrated strength.

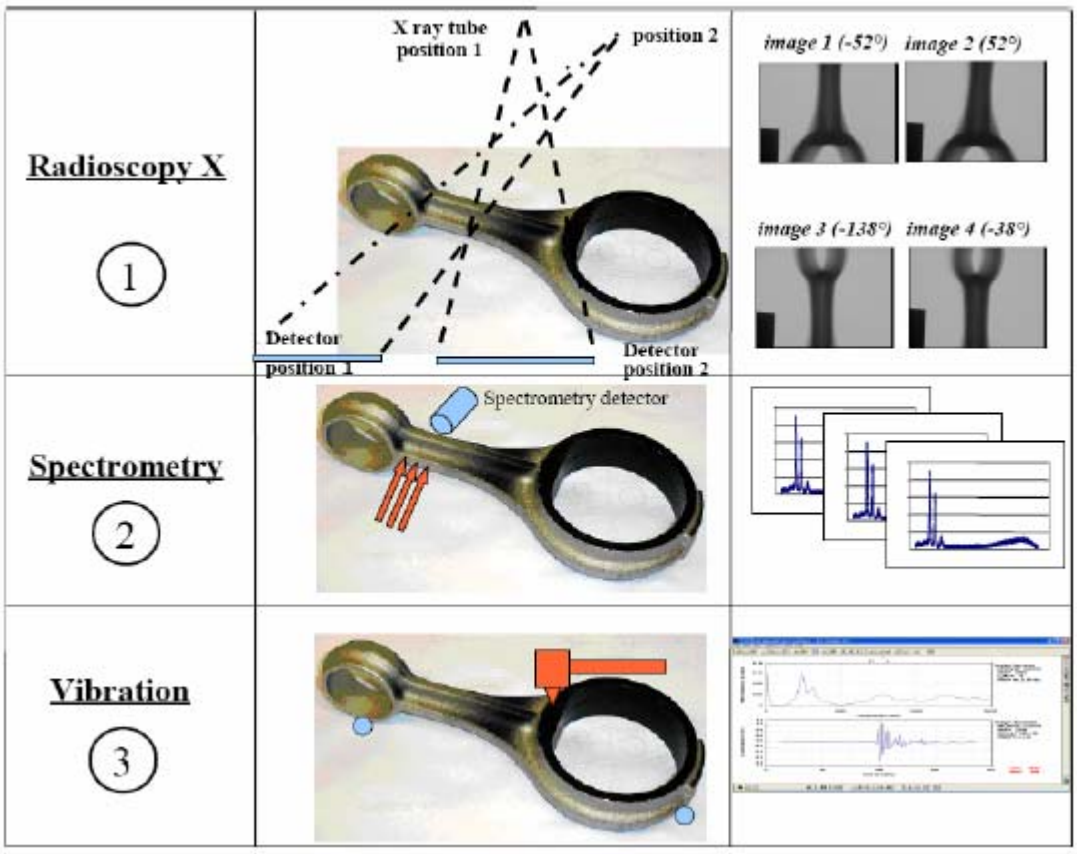


Figure 2 : The three acquisition steps and the corresponding output data.

*Data processing*

*Radioscopic data*

Radioscopic images are segmented using an automatic image processing routine developed under Matlab software. The image processing is based on the morphological top hat filter, after a noise reducing step. The top hat is followed by an hysteresis thresholding. Regions of interest are selected from the grey-level histogram by a K-means algorithm . This stage makes the routine potentially adapted to radioscopic images of more complex castings, providing that the number of regions of interest is a priori known. The routine is described in [2].

Image processing is followed by feature extraction, where mean grey-level, standard deviation, contrast to noise ratio, area, position, are measured for each object. Those

features allow to compute a confidence level in the hypothesis that the object is potentially a defect (see section 3.2.1).

*Spectrometry data*

Three spectra are extracted for the three volumes selected in the critical zone (see figure 2 to see the location of the measurement volumes). The total number of photons is normalised using the two reference measurements done between each acquisition. The normalised measurements are compared to average and standard deviation calculated from measurements of samples without defect in this particular area.
The possibility of extracting only the low energy part of the spectra was investigated by the RISOE partner. The enhancement of contrast expected is balanced by the decreasing of the number of counts, and due to the acquisition time constraints, it was decided to keep the whole spectrum.

*Vibration data*

The acquisition methodology for this method, as well as the data processing, were developped in the frame of the QUME project by The University of Liverpool [3] and MONITION company.
A neural network was trained on a set of samples without defects. Then, for each new sample, the neural net output is compared to the typical output computed from the normal samples. The Mahalanobis distance is chosen as a parameter to assess the potential defect presence in the whole sample. The dispersion of the eleven successive values obtained for each sample will be used to evaluate the reliability of the method.

The Figure 3 summarizes the data processing steps of the three techniques. It is worth noting that the type and number of data are different for each method :

- radioscopy delivers four images of the same sample, inside which several defects can be detected, featured by the list of their parameters (contrast, area, etc...);
- spectrometry delivers 3 measurements for a given sample, featured by the normalised number of counts for the three considered positions;
- vibration analysis delivers 11 measurements (successive in time) relating to the globality of the sample.

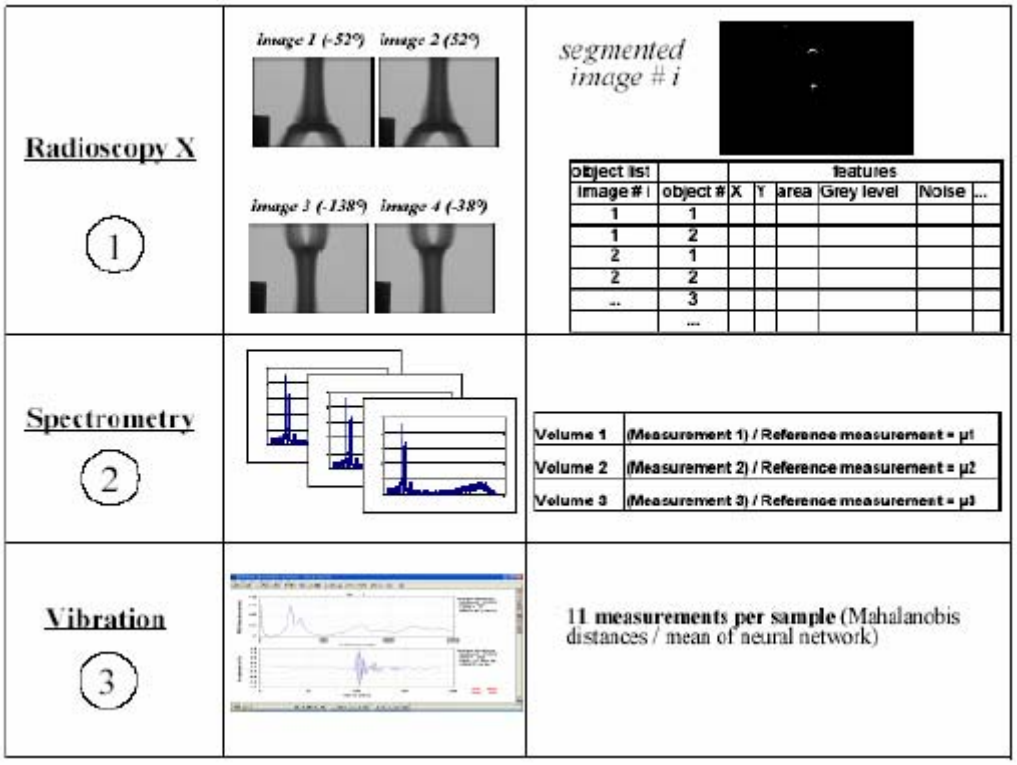


Figure 3 : Data processing for the three methods.

This means that data will have to be combined at different levels :

- radioscopic objects can be fused together if a geometrical matching is done to check their correspondance;
- spectrometric volumes can be fused with radioscopic objects, if some have been detected in those spectrometric areas;
- vibration data can only be fused at the level of the whole sample, so that X-ray data must first be summarized into a global information.

**Data Fusion with the Evidence Theory**

Data fusion refers to an automatic combination of information issued from different measurement techniques in order to get a more complete information and improve reliability.
It is useful for any application when only one technique is not sufficient to get all the required information. In this case, the complementarity of the different techniques is a key point, and data fusion consists in gathering the information given by the respective techniques.
Should one method only be able to make the measurement, but with a given uncertainty, it is also worthwhile to use another measurement technique to confirm the information. In this case, the techniques have a part of redundancy, but the use of both enhances reliability of measurement. Here, data fusion is not just "adding" information, in this case, it is a real combination. Complementarity and redundancy of the data sets are the basis of any data fusion application.
In our case, the two X-ray methods deliver an attenuation measurement, which is essentially redundant. However, their detection performance should depend on the sample thickness in a complementary manner. As far as vibration analysis is concerned, difficult defects such as cold junctions are hoped to be potentially detected. It is expected that the reliability of the measurement can be enhanced by the joint use of the 3 methods.

Data fusion methods can be used at image level, on a pixel by pixel basis, which is referred to “low level” data fusion. When data are first processed before being combined, one speak about “high level” data fusion, which is our case.

*Overview of the use of data fusion in NDT applications*

The use of elaborated techniques of fusion appeared around 1994 in the field of NDT [4,5,6]. Until this time and still now in a number of applications, when several inspection systems are used, the combination is done manually by the expert.

X.E Gros [7] developed a fusion between eddy current and ultrasonic systems applied to the characterisation of artificial weld defects, using the Bayesian inference and the Dempster-Shafer theory. Quantitative and qualitative data fusion at both high level and pixel level were performed. It has been shown that Bayesian approach is very dependent upon sensor efficiency and knowledge of a measurement, and does not always allow decision making. The theory of evidence appears more adequate when information from multiple systems is combined, and does not require prior knowledge of a measurement. Ultrasonic and X-rays are often used together in particular for weld inspection, and thus, several attempts of data fusion are found for these techniques. In [8], a 3D approach is reported to provide the inspector a tool that brings out the nature (volumic or not) and the direction of a defect inside an inspected piece. The aim is to help the inspector in making decision. Both probabilistic and evidence theory approaches have been tested. The evidence theory showed better results in defect positioning and sizing compared to probabilistic approach. Following of the work is also reported in [9] where Dempster-Shafer evidence theory was selected to fuse X-ray and ultrasonic data for weld inspection. In this application, fusion is done at the pixel level. Another approach is presented by our team in [10] for weld inspection as well, where high level fusion was chosen. Both projects were working together in the frame of an European thematic network, this joint work was presented in [11].
For other NDT techniques, few attempts of data fusion are reported in the field of aircraft industry between ultrasounds and shearography [12], or for Civil Engineering and Electronic inspection[13]. This brief survey shows that Evidence theory appears adequate for NDT applications, although data fusion is not yet widely used in this field.

*Dempster-Shafer theory*

Dempster-Shafer (DS) evidence theory was developed as an attempt to generalise probability theory [14,15]. It is suitable to reason with uncertainty and has been developed to overcome the limitation of conventional probability theory by distinguishing between uncertainty and imprecision. This is achieved in particular by making it possible to handle composite hypotheses. In DS theory, there is a fixed set of N mutually exclusive and exhaustive elements, called the frame of discernment, which is symbolised by $\Theta = \{H_1, H_2, \ldots, H_N\}$. $\Theta$ defines the working space for the application being considered since it consists of all propositions for which the information sources can provide evidence. In our case, only two hypotheses are considered : $H_1$ which can be 'there is a defect' or 'the sample is bad', and $H_2$ : 'there is no defect' or 'the sample is good'.

Information sources can distribute mass values on any subset of the frame of discernment, *i.e.* either on a single hypothesis $H_i$ or union of single hypotheses (composite hypotheses). That is, if an information source can not distinguish between two propositions $H_i$ and $H_j$, it

assigns a mass value to the set including both propositions ($H_i \cup H_j$). The ability to assign mass function to composite hypotheses is one of the important advantages of this theory, because it allows to model an hesitation between two hypotheses (for example two different types of defects can have the same appearance in an X-ray image). For our simplified case involving only two hypotheses, only one union is possible, representing the total ignorance. In the following, $A_i$ represent any subset of $\Theta$, i.e. either $H_1$, $H_2$ or $H_1 \cup H_2$.

The mass distribution for all the hypotheses has to fulfil the following conditions:

$$m(\phi) = 0 \qquad \text{and} \qquad \sum_{A_i \in 2^\Theta} m(A_i) = 1$$

Mass distributions $m_1$, $m_2$ from two different information sources are combined with Dempster's orthogonal rule. The result is a new distribution, $m = m_1 \oplus m_2$, which carries the joint information provided by the two sources:

$$m(A_i) = (1-K)^{-1} \times \sum_{Ap \cap Aq = A_i} m_1(A_p)\, m_2(A_q) \tag{1}$$

where : $$K = \sum_{Ap \cap Aq = \phi} m_1(Ap) m_2(Aq) \,. \tag{2}$$

K is often interpreted as a measure of conflict between the two sources and it is introduced in relation (1) as a normalisation factor. The larger the K value, the more conflicting the sources and the less sense their combination. From a mass distribution, two functions can be evaluated that characterise the uncertainty about the hypothesis $A_i$: the belief function Bel (also called credibility) measures the minimum uncertainty value about $A_i$ , whereas plausibility Pls reflects the maximum uncertainty value about this hypothesis. These two measures span an uncertainty interval [Bel($A_i$), Pls($A_i$)], which is called "belief interval". The length of this interval gives a measurement of imprecision about the uncertainty value. Belief and plausibility functions are defined from the set of symbolic set of hypotheses $2^\theta$ to the unit interval [0, 1]:

$$Bel(A_i) = \sum_{A_j \subseteq A_i} m(A_j) \qquad Pls(A_i) = \sum_{A_j \cap A_i \neq \phi} m(A_j) \tag{3}$$

The belief of the event $H_i$ is thus the sum of the likelihood of the events $A_j$ that validate the potential decision $H_i$, while the plausibility represents the sum of the likelihood of the events that do not deny the potential decision $H_i$.

*Mass value estimation*

The estimation of mass distributions is a known difficulty of the Dempster-Shafer theory, in the sense that no indication is given to the user, which means on the other hand that the user is free to choose the distribution best fitted to his knowledge on the data. We developped a mass value estimation for radioscopic images, which can be generalized to the three types of measurements.

X-rays transmitted by a given thickness of matter follow a normal law distribution, where the variance equals the mean. This means that, for a sample without defect, the grey-level is expected to follow a gaussian distribution. The standard deviation of the grey-level might not be exactly the quantum noise if the detector noise is not negligible. Nevertheless, the normal distribution is respected, with the standard deviation and mean measured on the grey-levels of an homogeneous thickness of matter.

The contrast to noise ratio measured on an object reflects to what extent the grey-level of the object is far from the mean value of an homogeneous thickness, as compared to the standard deviation. This is the basis of the following relation, which defines the mass of the « defect » hypothesis $H_1$, or the confidence level assigned to the fact that the object is potentially a defect. The term « *Measure* » refers to the information available on the object, namely its grey-level as far as radioscopy is concerned. *m* and *s* are respectively the mean and standard deviation of the distribution of the measurements in a sample without defect.

$$m_{Method}(H_1) = 1 - exp\left(\frac{-(Measure-\mu)^2}{(\alpha 2(\sigma)^2)}\right) \quad (4)$$

*a* is a weighting factor which is used to adapt the mass distribution to the reliability of the method itself, i.e., the confidence we have on the method.
The Figure 4 illustrates the mass obtained with a weighting factor a = 1 or 2.

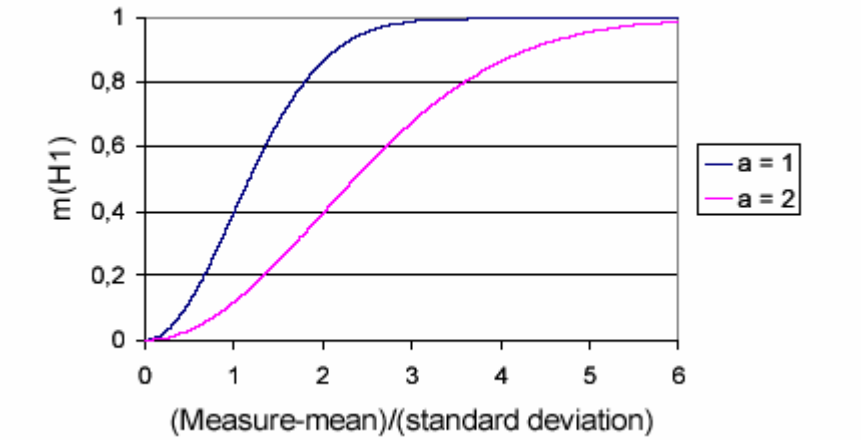


Figure 4 : Mass obtained in the hypothesis « defect », using the relation (4) with a weighting factor of 1 or 2.

For a = 1, one can see that the mass obtained is maximal for a deviation to the mean greater than 3s. a = 2 corresponds to a more cautious modelling, as a confidence level of about 70% is assigned for a deviation of 3s.
The complement to 1 is assigned to $m(H_3=H_1 \cup H_2)$, i.e., the ignorance level. This reflects the fact that a low deviation (measure – mean) with respect to the noise could either be a small defect indication (hypothesis $H_1$ « defect ») or a normal measurement (hypothesis $H_2$ « not a defect »).
If a specific knowledge is available for a measurement method relative to the hypothesis $H_2$ « this is not a defect », it is possible to assign it, provided that the global sum of the masses is 1.

*Fusion organisation*

To combine the three measurement results, a fusion in three steps is organised, as illustrated in the Figure 5 below.

- Step 1 : Each sample yields 4 radioscopic images, each of them potentially including several objects detected by image processing. Matched objects get their masses fused, thus delivering a global list of objects and associated masses.
- Step 2 : The same sample yields 3 X-ray spectra, measured for the 3 specific volumes (fig.2). If a radioscopic object matches one of the volumes, a combination of masses is performed.

At the end of this step, a global assessment of the mass values related to the sample is carried out.

- Step 3 : 11 vibration spectra are performed for the sample, all corresponding to the whole sample (the 11 spectra do not refer to 11 positions but 11 global spectra successive in time). Hence, no matching is necessary, and the mass values are simply combined at the sample level. The only difference is that the hypotheses become $H_1$ « bad sample » and $H_2$ « good sample ».

It is worth noting that the Dempster rule of combination also involves the computation of the conflict K (relation (2)). The K value is kept in memory in order to be considered in the decision stage.

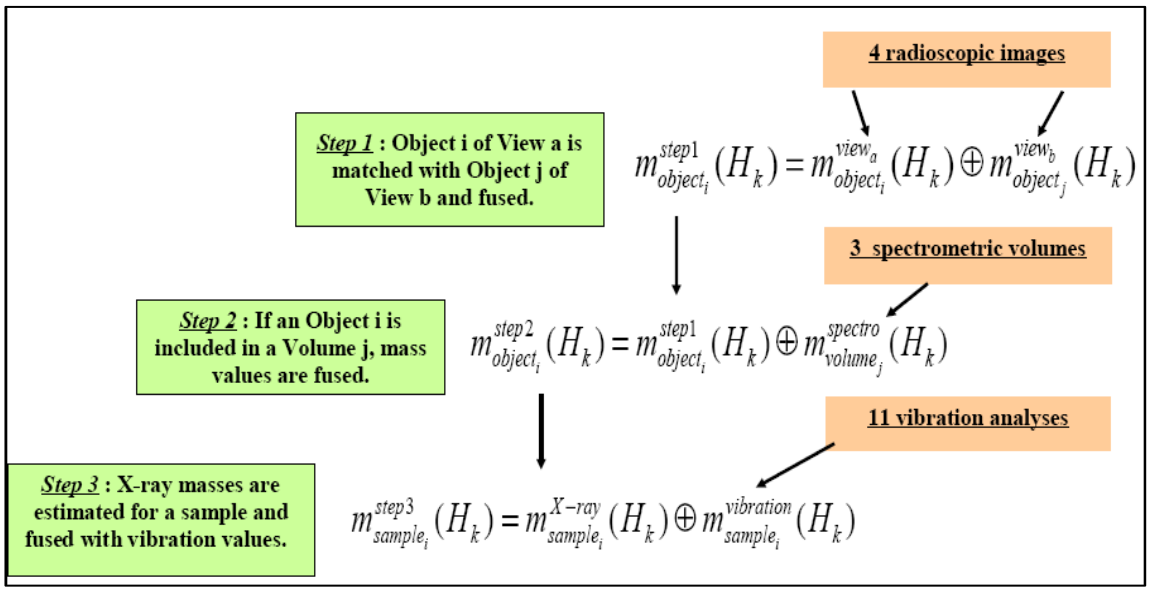


Figure 5 : Schematic diagram of the 3 fusion steps for one sample. The symbol ⊕ refers to the Demspter rule of combination (relation (1)).

## Results

Before developping step by step the complete process, the geometrical matching necessary for fusion is presented.

*Geometrical matching between detected objects*

*Geometric bench model*

Any detected object is the projection of an indication (true defect or not) in the sample. Hence, the real indication belongs necessarily to the straight line □, joining the X-ray source S and the detected object P (Figure 6).

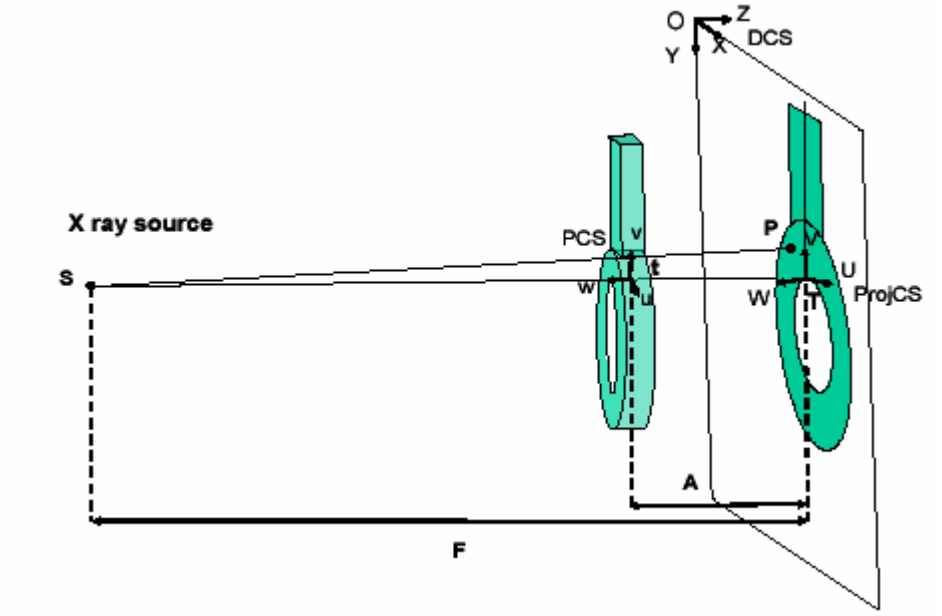


Figure 6 : Representation of the radioscopic bench, with three coordinate systems.

To be able to match objects detected in two images of different orientations, it is necessary to express the Δ coordinates in a common system. The piece coordinate system PCS was naturally chosen. Two other direct orthonormal systems are defined, the detector coordinate system DCS and the projected coordinate system ProjCS (figure 6).
Changing coordinates from one system to another is done with matrices, thanks to the homogeneous coordinates, which allow to express all the transformations (translation, rotation, homothetic) with 4x4 matrices.

*Geometrical matching*

Given two detected objects $P_1$ and $P_2$, the coordinates of the two lines $\Delta_1$ ($S_1$,$P_1$) et $\Delta_2$ ($S_2$,$P_2$) are calculated in the PCS and the distance ($\Delta_1$, $\Delta_2$) is calculated (Figure 7).

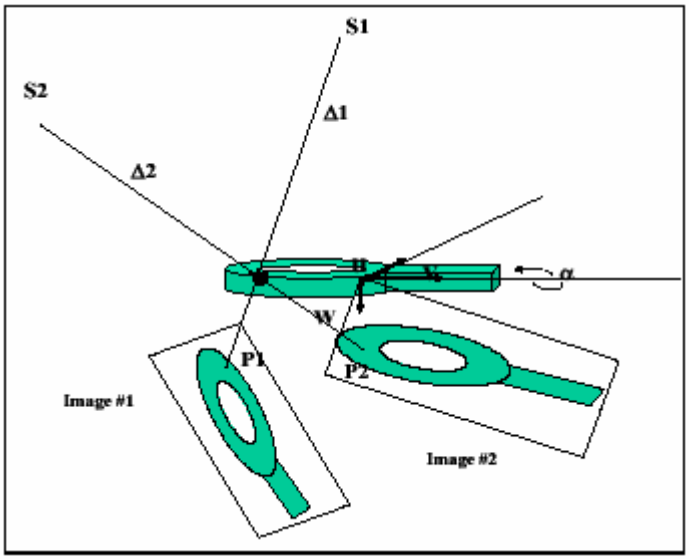


Figure 7 : Representation of the two lines Δ (S,P) for a sample, depending on the radiographic orientations.

The distance is compared to the maximal detected object dimensions (length), taking into account the uncertainty of all parameters. If the distance is inferior to the length, the two detected objects are assumed to be a single one.

All the dimensions and angles are measured with their respective geometric uncertainties, due to the mechanical angles accuracies during acquisition, the sample positioning giving a piece tilt in the image, the measurement and calculations uncertainties. Uncertainties thus derived are :

- a 0.7 mm radius sphere for any point position,
- a 2.25 mm radius sphere for any distance between a point and a line,
- a 2.5 mm radius sphere for any distance between two lines.

*Matching performance as measured on radioscopic detected objects*

The results of the matching is presented in the Table 1 :

*Table 1 : Matching results between radiographic detected objects from the 171 samples.*

| **Detected objects** | ***839*** | | |
|---|---|---|---|
| | **Defects** | **FA** | **Total** |
| **Matched objects** | 42 | 657 | 699 |
| **Matching couple number** | 33 | 558 | 591 |
| **Non-matched objects** | 17 | 123 | 140 |

699 detected objects are matched, among them 42 are true defect projections, and 657 are false alarms (FA).
The case of FA needs a comment. It could be surprising at first glance, because FA are usually due to noise detection. In our case, those FA are systematic, and have been analysed as coming from a particular zone of the sample. Due to the orientation of the sample rings, the thickness change induces a grey-level variation which is detected by the image processing. These systematic FA are thus always located at the same place, which is close to the point T (origin of ProjCS). In order to « mark » these particular objects, a geometric feature was defined as the distance Dt between the line Δ and the point t. Systematic FA exhibits a Dt inferior to 10 mm. In the section 3.2.1, this feature is used to assign a confidence level to the hypothesis $H_2$ « this is not a defect ».

The matching couple number is greater than half the number of matched objects. Indeed, one detected object in view #i can be matched to several other detected objects in view #j. For example, systematic FA can be detected in one or two fragments in the same area. In that case, one single object of view #i can be matched with the two objects of the other view. Few samples contain a defect in the central arm, which is detected in three or four views. In that case one global object is concerned by two or three matching couples.

The geometric bench model developped for this study is very efficient. All the 591 matchings are performed between objects of same type (defect/defect and FA/FA) without any error, showing the performance of the calculation method. Moreover, the geometric model allows to compute a distance measure, allowing to distinguish systematic FA located at a specific position.It must be said however that, although no matching is done between a defect and a FA, it remains possible if a defect occurs in the area of the T point. This is fortunately unlikely to happen, as the t point is on the external border of the sample, and its projection T is still on the sample image boundary. The threshold distance chosen at 10 mm in the projection corresponds to a dead zone for the defect detection.

*Fusion step 1 : radioscopic objects in view #i ⊕ radioscopic objects in view #j*

*Mass values*

Each detected object is assigned a mass value for the hypothesis $H_1$ according to relation (4), where the Measure is the mean grey level (GL) of the pixels constituting the object. m and s are respectively the mean and standard deviation of the grey-levels of the object neighbourhood. Thus, relation (4) can be expressed using the Contrast to Noise Ratio (CNR) of the object and its neighborhood (relation (5).

$$m^{view\,a}(H_1) = 1 - \exp\left(\frac{-CNR^2}{2}\right) \quad (5)$$

The $H_3$ mass is the complement to 1 of $m(H_1)$ : $m^{view\,a}(H_3) = 1 - m^{view\,a}(H_1)$

This first estimation is based only on the grey-level distribution of the object and its neighborhood.
Other information can also be taken into account for the hypothesis $H_2$ « this is not a defect », which in our case means « this is a FA ». As explained in the previous paragraph, a geometric feature allows to classify correctly systematic FA.
On the other hand, the manufacturer has an acceptability level according to the size of the detected objects. Objects with an area inferior to 1 $mm^2$ in the radioscopic image are not considered critical. It was also explained in [2] that all the detected objects with GL superior to a value $GL_0$ were FA.
To summarize this knowledge, any detected object will get $m^{viewa}(H_2)=1$, (and thus $m^{viewa}(H_1)=0$ and $m^{viewa}(H_3)=0$) if :

- its area is inferior to 1 $mm^2$,
- and/or its grey level is superior to $GL_0$,
- and/or its distance Dt is inferior to 10 mm.

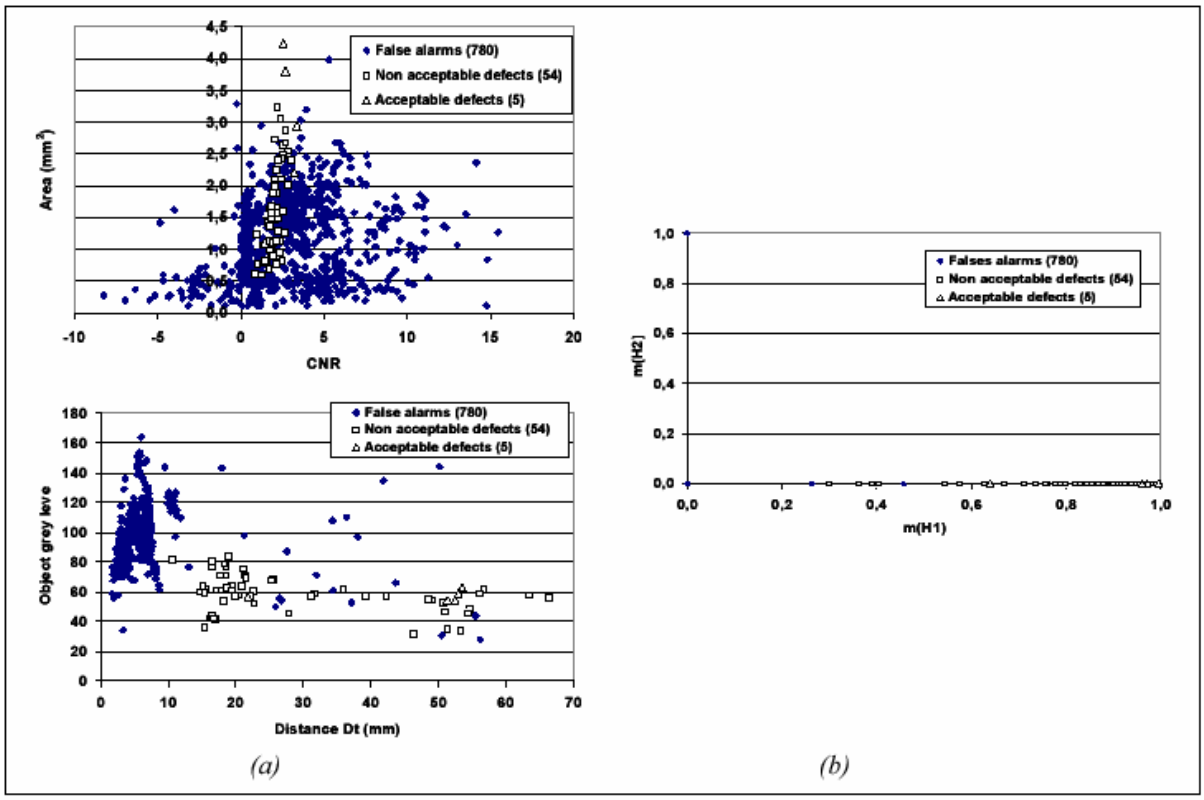


Figure 8 : Representation of features of the detected objects (a) the area versus CNR and the object grey level versus the distance Dt and for the same objects (b) m(H2) versus m(H1).

The Figure 8a shows the features of the detected objects (CNR versus area, and GL versus distance Dt), where one can see that a direct discrimination of true defects and FA is not trivial. The Figure 8b shows the $m(H_2)$ versus $m(H_1)$ graph, where it appears that true defects get a confidence level in the defect hypothesis (although not very high for some of them if low contrasted) and most FA get a mass value of 1 in the $H_2$ hypothesis, as well as acceptable defects.
Thus, the knowledge we have on the features is well translated in the mass values.

*Fusion*

As explained in table 1, 591 object couples are matched, including 33 true defects.

As visible on figure 8, thanks to the mass estimation, no ambiguity remains on the object nature, systematic FA or defect (as most of the FA all have a $m(H_2)=1$). Few defects get a mass value in the $H_1$ hypothesis which is not very high. For them, it is expected that the fusion step will increase the confidence level (i.e. credibility or belief in the defect hypothesis).

The mass improvement for the 33 defects is of 4% on average. The following figure shows an example of three fusion results : case 1 reflects the case of a middle confident defect in view a, which is detected with a better confidence in view b, and thus, the combination results in a perfect credibility in the end; case 2 and 3 show also an improvement, although the confidences are already high in each view.

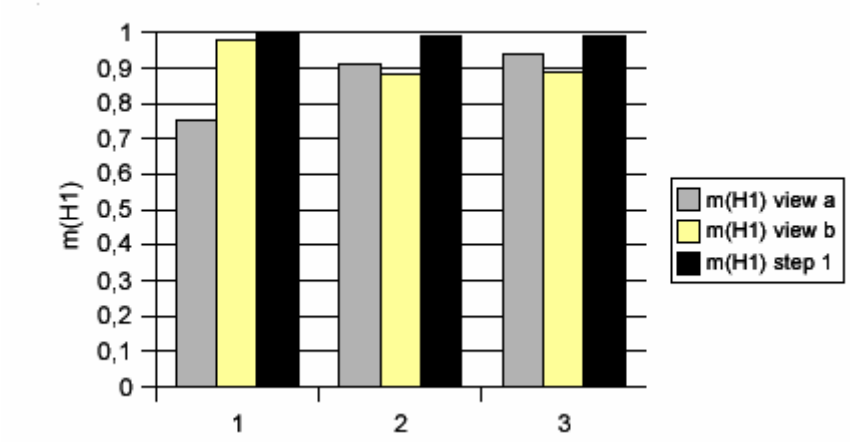


Figure 9 : Fusion step 1, examples of three fusion results.

*Fusion step 2 : radioscopy ⊕ spectrometry*

*Spectrometry mass values*

Spectrometry measurements for good and bad samples were analysed prior estimating the masses (fig.10). Samples indicated « with possible defects » refer to pieces where the manual test revealed a defect located in one of the volumes where a spectrum is measured. Unfortunately, the location reported by the manual test was not very accurate, this is why we mention « possible defect ».

The mean $\mu_{spect}$ and standard deviation $\sigma_{spect}$ are calculated for samples without defect. Some samples with defects get a measurement clearly far from $\mu_{spect}$, however, few samples without defect have measurements superior to $(\mu+3\sigma)$.

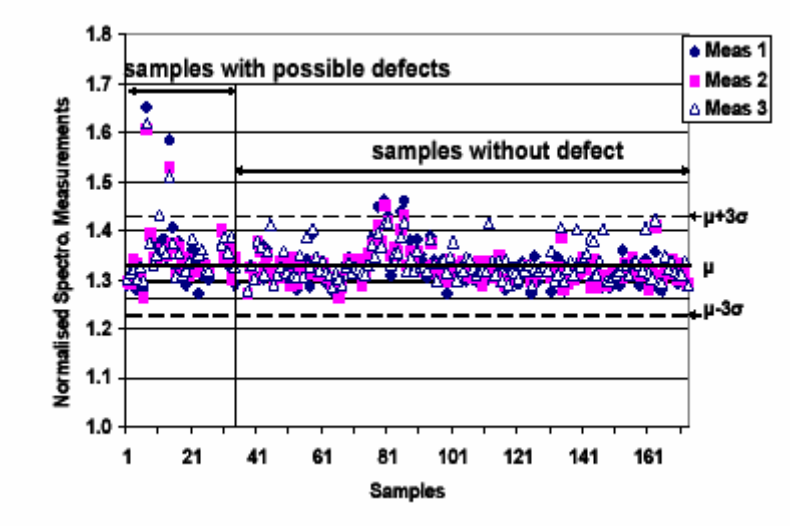


Figure 10 : Three spectrometric measurements done for each sample, after the normalisation with reference thickness values.

Hence, a cautious mass estimation was done with an α coefficient of 2 in relation (4), which becomes relation (6) :

$$m^{spectro}(H_1)=1-\exp\left(\frac{-(N_{spect}-\mu_{spect})^2}{(2.2(\sigma_{spect})^2)}\right)$$

$$m^{spectro}(H_3)=1-m^{spectro}(H_1) \quad \text{which gives} \quad m^{spectro}(H_2)=0 \qquad (6)$$

Once applied to the previous measurement values, the obtained masses are plotted on Figure 11.

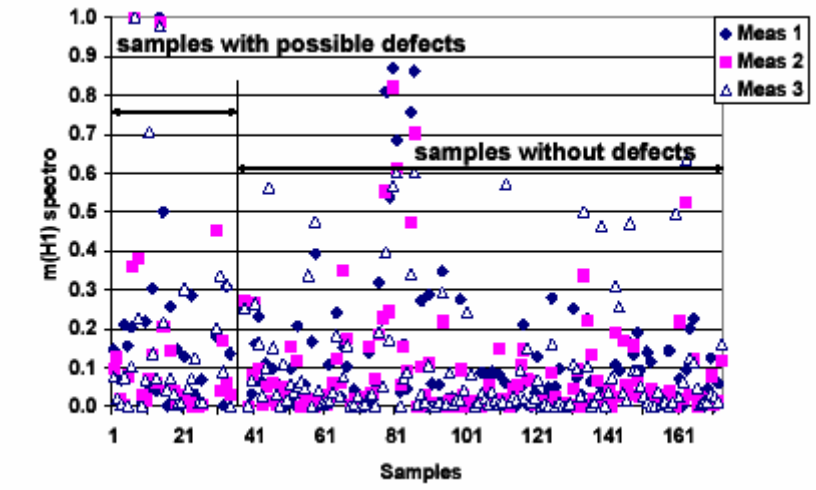


Figure 11 : spectrometric m($H_1$) evaluation done with the normalised measurements of the Figure 10.

*Fusion*

32 radioscopic objects are matched with 32 spectrometric volumes. No matching occured with any FA. Five different examples of fusion are showed in the following figure :

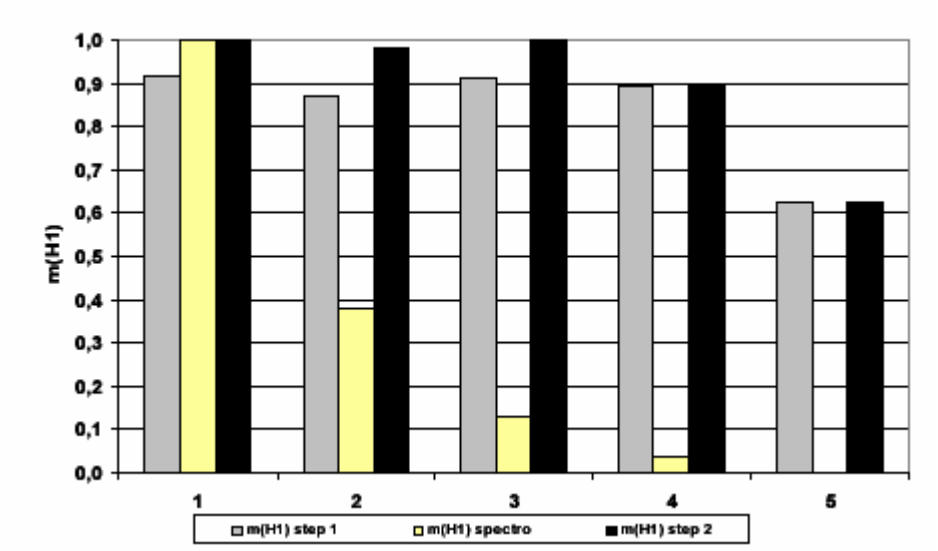


Figure 12 : Second step fusion : results of m ($H_1$) combination radioscopic objects □ spectrometric volumes, after matching.

When there is a matching, the combination improves the $H_1$ mass, i.e. the defect confidence. This is a good result. Unfortunately, the problem of spectrometric results is that good samples also get a mass in the hypothesis $H_1$, which means that those results are not enough reliable if used alone. For this reason, if there is a combination with radioscopy, we consider the combination, but if spectrometry detects an indication, without radioscopy, the result is not considered.

The complementarity of the spectrometric control is not obtained. The main reason was the positionning accuracy of the sample, which is unsufficient to warrant a reproducible thickness measured.

*Fusion step 3 : X-ray ⊕ vibration*

Before this fusion step, masses relating to the global sample must be defined from the masses of the objects contained in it. We consider that the defect having the highest mass in $H_1$ gives its criticity to the sample. On another hand, at the sample level, the $H_2$ hypothesis 'this is not a defect' becomes 'the sample is good'.

*Vibration mass values*

For assigning vibration masses, the relation (4) is used and becomes (7), where the mean value $\mu_{vib}$ is obtained from a group without defect, as well as the standard deviation $\sigma_{vib}$. . The measure $N_{vib}$ refers to the output of a neural network, which is expressed as the Mahalanobis distance of the neural net output with respect to the learning set containing only good samples. Thus, the mean value measured on good samples $m^{vib}$ should be null, but indeed the measurement during the learning and after were different.

$$m^{vib}(H_1)=1-\exp\left(\frac{-(N_{vib}-\mu_{vib})^2}{(2(\sigma_{vib})^2)}\right) \quad ; \quad m^{vib}(H_3)=1-m^{vib}(H_1) \quad ; \quad m^{vib}(H_2)=0 \tag{7}$$

Vibration results are shown in the Figure 13. Unfortunately, no clear difference appears between the good and bad samples. At this stage of the vibration control setting, the

combination is useless and fusion was not performed.

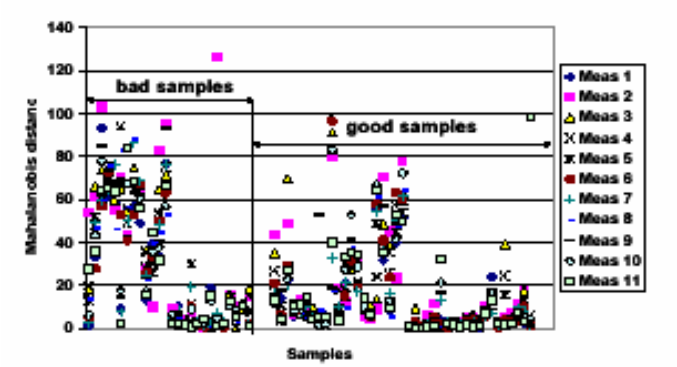


Figure 13 : Eleven vibration measurements for each sample.

## Final decision on sample acceptability

In the case of two hypotheses, relations (3) are simplified. The credibility or belief of $H_1$ is equal to its mass. The decision criterion chosen is the maximum of belief between $H_1$ or $H_2$, providing that the conflict is small.

31 samples have a non null $H_1$ credibility (Figure 14). Among them, 27 are said unacceptable by the manufacturer, two samples have acceptable defects and two are good samples. If a threshold on the belief is defined, for example 0.6, only defectuous samples are rejected.

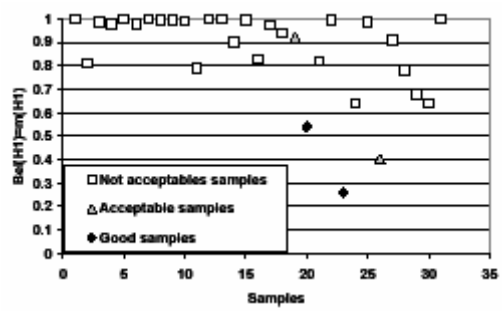


Figure 14 : Plot of the 31 samples having a belief in the $H_1$ hypothesis , labeled with the end user acceptability

The other 140 samples have a credibility of $H_2$ equals to 1. Among these samples three have unacceptable defects (cold junction and inclusion), which were not detected by the radioscopic control as expected. Unfortunately the other measurement techniques did not detect them as well.

With the decision threshold of 0.6 on the belief, the global performance obtained on the 171 samples is thus a probability of detection of 90 % (=27/30) and probability of false rejects of 0.7 % (=1/140). Besides, the only false rejected sample contains really a defect, which means that our automatic inspection is slightly more severe than the manufacturer control.

## Conclusion

A fusion approach was presented to combine data from different NDT modalities. The concept of confidence level defined in the Evidence Theory is used, and our contribution is on the definition of mass values which is generalized to the 3 measurement techniques. A weighting factor allows to adapt it to the reliability of the results.
The combination of X-ray images is very efficient. Some defects would be missed with only one projection, and matched defects in different views get their confidence higher. Thus, complementarity and redundancy of information is helpful. The matching is a crucial step, as it induces the performance of all the combination. Our geometric bench model is robust and takes into account the uncertainties of the acquisition stage.
Unfortunately, spectrometry did not show the sensitivity expected, and thus a cautious fusion is adopted. Vibration analysis results were not reliable enough to allow a successful data fusion step, but this can be considered normal when an innovative method is introduced. Nevertheless, the potential of the global fusion approach is validated.

Whatsoever, the automatic inspection presented here is validated on 171 samples with a performance of 90 % in true positive detection and 0.7% of false rejects rate, which is very encouraging.

## Acknowledgements

This work was performed as part of the project Qume G1RD-2000-00444, funded by the European Community. The authors would like to gratefully acknowledge Mrs Paola Giordano (Stampal S.p.A.) for supplying aluminium cast components and X-ray manual analysis, and the entire Consortium for their interest in the projet.

## References

[1] CENDRE E., KAFTANDJIAN V., LECOMTE G., KJAER K. Complementarity of a photon-counting system and radioscopy for inspection of cast aluminium components. NDT&E International (38) 2005, pp. 239-250.
[2] LECOMTE G., KAFTANDJIAN V., CENDRE E., BABOT D. A robust segmentation approach based on features analysis for defect detection in aluminum castings X-ray images. NDT&E International, submitted June 2005.
[3] WONG M.L.D., JACK L.B., NANDI A.K. Modified self-organising map for automated novelty detection applied to vibration signal monitoring. Mechanical Systems and Signal Processing, 2005, accepted, 18p.
[4] GEORGEL B., LAVAYSSIERE B. Fusion de données : un nouveau concept en CND. In : Proc. of the 6th European Conf. on NDT, vol. 1, 1994, p.31-36.
[5] GROS X.E., STRACHAN P., LOWDEN D.W., EDWARDS I. NDT data fusion. In : Proc. of the 6th European Conf. on NDT, vol 1, 1994, p.31-36.
[6] JOHANNSEN K., HEINE S., NOCKEMAN C., FILBERT D. New data fusion techniques for the reliability enhancement of NDT. In : Proc. of the 6th European Conf. on NDT, vol 1, 1994, p.361-365.
[7] GROS X.E. NDT Data fusion, John Wiley and Sons, New York, 1997, 205 p.
[8] LAVAYSSIERE B. Fusion de données radiographies et ultrasonores. Journée de radiologie industrielle JRI' 97, Grenoble, 1997.
[9] FRANCOIS N. A new advanced multi technique data fusion algorithm for NDT. In :15th WCNDT, Roma, 15-20 October, 2000.
[10] DUPUIS O., KAFTANDJIAN V., ZHU Y.M., BABOT D. Détection de défauts par fusion de signaux ultrasonores et d'images radioscopiques. In : 17°colloque GRETSI, Vannes, France, 13-19 september, 1999.

[11] KAFTANDJIAN V., FRANCOIS N. Use of data fusion to improve reliability of inspection : synthesis of the work done in the frame of a European Thematic Network. In : Proc. of the 8th ECNDT, Barcelona, 17-21 June, 2002.
[12] MATUSZEWSKI B. J., SHARK L. K., VARLEY M. R. Region-based wavelet fusion of ultrasonic, radiographic and shearographic non destructive testing images. In : Proc. of the 15th WCNDT, Roma, 15-20 October, 2000.
[13] GROS X.E. Applications of NDT Data fusion, Kluwer Academic Publishers, 2001, 277 p.
[14] DEMPSTER A. Upper and lower probabilities induced by multivalued mapping, Annals of Mathematical Statistics, 1967, vol. 38, pp. 325-339.
[15] SHAFER G. A mathematical theory of evidence. Princeton University Press, 1976, 297 p.